Angle-resolved secondary photoelectron emission from graphene interfaces

Oleg Yu. Vilkov,[1,*] Eugene E. Krasovskii,[2,3,4] Alexander V. Fedorov,[5] Artem G. Rybkin,[1] Alexander M. Shikin,[1] Clemens Laubschat,[6] Jorge Budagosky,[3] Denis V. Vyalikh,[3,4] and Dmitry Yu. Usachov[1]

[1]*St. Petersburg State University, 7/9 Universitetskaya nab., St. Petersburg, 199034, Russia*
[2]*Departamento de Física de Materiales, Facultad de Ciencias Químicas, Universidad del Pais Vasco/Euskal Herriko Unibertsitatea, Apdo. 1072, 20080 Donostia/San Sebastián, Basque Country, Spain*
[3]*Donostia International Physics Center (DIPC), Paseo Manuel de Lardizabal 4, 20018 Donostia/San Sebastián, Basque Country, Spain*
[4]*IKERBASQUE, Basque Foundation for Science, 48013 Bilbao, Basque Country, Spain*
[5]*IFW Dresden, P.O. Box 270116, 01171 Dresden, Germany*
[6]*Institute of Solid State and Materials Physics, Technische Universität Dresden, 01062 Dresden, Germany*

Angle-resolved secondary electron emission spectra were analyzed for studying the electron transmission properties of graphene when it is tightly bound to a metallic substrate and when it is decoupled from the latter. As respective model systems, graphene/Ni(111) and graphene/Au/Ni(111) were considered. We discovered two types of spectral structures linked with the transmission properties of graphene: bands related to scattering resonances and to umklapp reflection. These findings are interpreted based on an *ab initio* theory of the scattering of the outgoing electrons by the graphene overlayers. The experimental secondary electron emission maps are in good agreement with the calculations, indicating that such approach can be successfully applied for studying the electron transmission properties of a variety of two-dimensional materials.

I. INTRODUCTION

Quasi-two-dimensional (Q2D) materials, such as graphene, silicene, hexagonal boron nitride, and transition metal dichalcogenides, as well as their various composites and heterostructures, have received much attention in the last years [1,2]. These materials are promising for applications in the emerging fields of nanoelectronics, spintronics, energy conversion and storage, catalysis, biosensors, etc., owing to the low-dimensionality, flatness, and unique transport properties of Q2D systems [3–7].

The information about electronic properties can be obtained experimentally by means of angle-resolved photoelectron spectroscopy (ARPES), allowing us to map the electron band dispersions. It is widely applied to different kinds of Q2D materials, where the main attention is paid to the analysis of the primary photoelectrons, providing insight into the fine electronic structure of the valence band, particularly near the Fermi level. This gives valuable information on the properties of the charge carries, their group velocity [8], concentration [9], spin texture [10], information on the charge transfer [11], many-body interactions [12], etc.

In the standard experiment, the spectral structure of the secondary electrons located mostly in the low-energy part of the ARPES spectrum is quite often overlooked or does not receive enough attention and discussion. At the same time, this part of the photoelectron spectra also contains essential information about the properties of the studied material. For example, this makes it possible to explore the electronic structure of unoc-cupied states near the vacuum level [13–16] or to investigate the electron transmittance of the Q2D system. In particular, the transmission coefficient $T(E)$ of graphene at low kinetic energies was studied with this method [17,18]. Note that ARPES studies of secondary electrons allow us to get unique information on the angular dependence of $T(E)$ or on the reflection coefficient $R(E)$, which are usually explored via the target current spectroscopy [19,20], very low-energy electron diffraction (LEED) [21,22], and angle-resolved low-energy electron transmission and reflection [23–25] methods. This, in turn, has enabled us to determine the thickness [26,27], homogeneity [28,29], crystallinity [17], and lattice parameters [18,30], and to recognize the Q2D systems to be functional and efficient in low-energy electron holography [31], field emission electron sources [32], or for optoelectronics and related areas.

In that regard, the most interesting features of electronic structures considerably influencing the $T(E)$ coefficients are the scattering resonances embedded into energy continuum. The existence of scattering resonances, i.e., quasistationary bound states with complex eigenenergies, has been shown theoretically for a single-atom-thick system, and in particular for graphene [33]. These states appear due to a strong coupling of the electron's motions perpendicular and parallel to the layer. The signature of such resonances has been obtained theoretically in simulations of the secondary electron emission spectra for suspended graphene [34] as well as experimentally in such spectra taken from graphene formed on different substrates [17,24,35]. But the most obvious confirmation of existence of quasistationary states was obtained in experiments with low-energy electron point-source microscopy. It was found that low-energy electrons with energy and momentum

*ol.vilkov@gmail.com

satisfying the resonance conditions undergo strong reflection [25]. This is clearly observed in the experimental data as a set of sharp minima in the angular dependence of the transmission function $T(E, \mathbf{k}_\parallel)$ for freestanding graphene.

Considering graphene formed on a substrate, it is reasonable to assume that certain features in the spectral pattern of secondary electrons will be determined by the transmission coefficient $T(E, \mathbf{k}_\parallel)$ of the graphene layer. Such a system can be thought of as consisting of two parts: the substrate, which acts mainly as a source of secondary electrons, and the graphene layer on its surface. The latter acts as a filter for the secondary electrons because of its strongly selective transmission properties. Then, the reasonable question arises: How and to what extent do the properties of the interface between graphene and substrate affect $T(E, \mathbf{k}_\parallel)$? Depending on whether graphene is strongly bound or only weakly coupled to the substrate, it may act differently as a filter for electrons.

Here, we address this point and evaluate in detail the properties of the transmission coefficient for graphene tightly covalently bound to the metallic substrate and for graphene experiencing only moderate interaction with the underlying material. In particular, we performed combined experimental and computational studies for graphene formed on nickel and on gold, reflecting the extreme cases of strong and weak coupling to the substrate, respectively. We studied the low-kinetic-energy ARPES spectra for both systems and compared them with calculations of $T(E, \mathbf{k}_\parallel)$ for freestanding graphene and graphene on a nickel surface. Our theoretical results are in a good agreement with the ARPES experiments. Additionally, we performed a comparative analysis of the bare metallic substrates Ni(111) and Au/Ni(111), i.e., without graphene layer on top. This allowed us to visualize and separate the substrate-related spectral features.

II. EXPERIMENTAL AND COMPUTATIONAL DETAILS

Graphene-based systems and bare metallic films were prepared *in situ* under ultrahigh vacuum (UHV) conditions. The base pressure in the UHV chambers was 2×10^{-10} mbar. Single-layer graphene was synthesized by chemical vapor deposition (CVD) on a crystalline Ni(111) film with a thickness of 12 nm deposited on a clean W(110) surface. The sharp (1×1) hexagonal LEED pattern of the Ni(111) film indicated its high crystallinity. The graphene synthesis was performed at substrate temperature of 600 °C and propylene (C_3H_6) pressure of 1×10^{-6} mbar for 15 min. Under these conditions, graphene growth on the hot metal surface lasts till the catalytically active metal is not passivated by a single graphene layer [10]. The obtained graphene was characterized by the hexagonal LEED pattern identical to that of the Ni(111) surface due to the close lattice parameters of graphene and Ni(111). Graphene was released from the tight chemical interaction with the substrate by the intercalation of gold atoms into the interface between graphene and Ni(111). Overlayer of gold with a thickness of 4 Å was deposited at room temperature on top of graphene/Ni(111) system with subsequent annealing up to 550 °C for 10 min. The thickness of the gold overlayer was monitored with a quartz microbalance. As a result of gold intercalation, a superstructure close to (10×10) appeared in the LEED pattern due to incommensurate lattice parameters of

graphene (nickel) and gold [36]. The samples of bare metallic films of Ni(111) and Au/Ni(111) were prepared as described above but skipping the CVD procedure.

ARPES spectra of graphene-derived systems were obtained at the U125/2-SGM beamline of the BESSY II synchrotron radiation facility (HZB Berlin) using the RGBL-2 station and linearly polarized radiation. The experiments with clean metallic films were performed at the resource center Physical Methods of Surface Investigation of Research Park of Saint Petersburg State University. In the latter case, a narrow-band UV He-discharge light source Scienta VUV 5k was used. All measurements were done with a hemispherical energy analyzer VG Scienta R4000.

To eliminate the effect of the contact potential difference between the sample and the analyzer, and to correct the measured kinetic energies of photoelectrons, we used the following values of the work function: 4.05, 4.56, 5.37, and 5.55 eV for graphene/Ni, graphene/Au/Ni, Ni(111), and Au/Ni, respectively [37,38].

The theory that relates the fine structure in angle-resolved secondary emission spectra with LEED was put forward by Feder and Pendry [39], and it was experimentally verified by Bovet *et al.* [40]. The original derivation [39] was based on thermodynamic considerations, and it can be understood by drawing on the one-step theory of photoemission, in which the transmission properties of the surface are included into the time-reversed LEED state $|\Phi\rangle$, i.e., the photocurrent in a given direction is proportional to the probability of the photoelectron to transfer to the $|\Phi\rangle$ state. For primary photoelectrons, the probability depends on the matrix element of the excitation operator. For secondary electrons, we are not in a position to calculate the true nonequilibrium distribution function; however, it is plausible to assume that the probability to occupy the $|\Phi\rangle$ state is proportional to the probability to find the particle in this state inside the solid. This probability is finite because the wave function $\Phi(\mathbf{r})$ decays into the interior of the crystal. This decay simulates the inelastic scattering of the photoelectron and is achieved by introducing the optical potential—the energy dependent imaginary potential $-iV_i$, which is spatially constant in the crystal and zero in the vacuum half-space. It can be shown [41] that this probability is proportional to the total current $T(E, \mathbf{k}_\parallel)$ carried by the $|\Phi\rangle$ state.

The LEED wave functions are obtained by solving the Schrödinger equation for the scattering of a plane-wave incident from the vacuum. For graphene on Ni(111), a semi-infinite geometry was adopted, in which the space is divided into three regions: the substrate half-space, where the potential is that of the bulk Ni crystal; the selvage region, where the potential gradually transfers from the periodic bulk distribution to the vacuum level; and the vacuum half space. The potential is taken to be the self-consistent one-particle potential of the density-functional theory in the local density approximation. In the surface layers, it is calculated as a potential of a finite-thickness slab, which comprises seven Ni layers and a graphene layer on each side of the slab. In the inner layers of the slab, it matches the bulk potential, and the graphene overlayer belongs to the fragment of the slab embedded between the semi-infinite bulk and vacuum. In the vacuum, the scattering wave function is given in terms of plane waves,
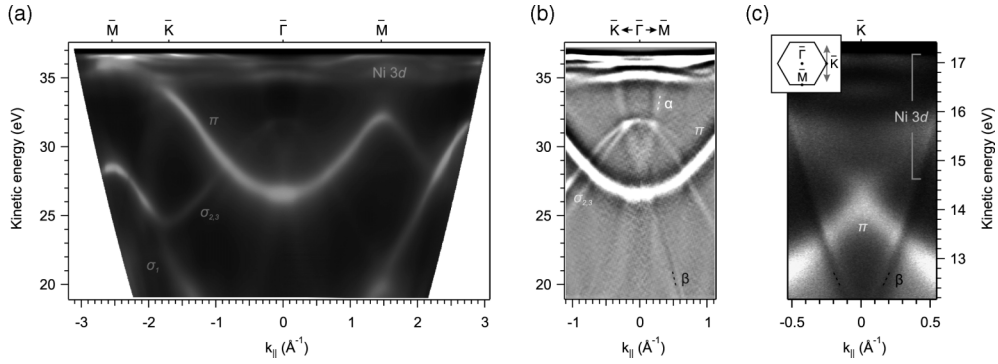
FIG. 1. ARPES-derived band structure of graphene coupled to the Ni(111) substrate measured along the high-symmetry directions. (a) As-measured survey intensity map depicted as $I(E, \mathbf{k}_\parallel)$. (b) The second-order derivative of the intensity map (a) taken near the $\bar{\Gamma}$ point and (c) the map $I(E, \mathbf{k}_\parallel)$ taken near the $\bar{K}$ point with the geometry shown in the inset. ARPES data were taken with $h\nu = 40.8$ eV (a), (b) and 21.2 eV (c).

and in the bulk it is a linear combination of Bloch solutions. The two representations are joined together continuously and smoothly at a boundary between the substrate and the surface using the variational method introduced in Ref. [42]. A similar procedure was used to calculate the electron transmission through a freestanding graphene layer, see Ref. [33].

III. RESULTS AND DISCUSSION

Figure 1(a) shows the electronic structure of graphene tightly bound to the nickel substrate measured with ARPES along the high-symmetry directions. The strong covalent bonding between C $2p_z$ and Ni $3d$ orbitals is reflected in a large shift of the graphene bands to higher binding energies by about 2–3 eV. Together with the π and σ states of graphene, the Ni $3d$ bands near the Fermi level are also well seen. However, a closer look at the spectrum near the $\bar{\Gamma}$ point reveals an additional spectral pattern, which was also seen in a previous study [17]. The respective $\mathbf{k}_\parallel$-range is shown in Fig. 1(b) as a second derivative of the ARPES intensity plot, where the mentioned spectral feature, labeled α, becomes better visualized. Another interesting feature is the black contour marked β. Its dispersion extends over all photoemission angles and is well seen at the $\bar{K}$ point [Fig. 1(c)]. In contrast to the highly intense features that stem from the π and σ states, the β feature is seen as a black contour, indicating a suppression of the ARPES signal.

Thus, in addition to the known valence band structure of graphene/Ni(111), there are other peculiarities of the ARPES spectra. One may assume that the α and β features appear due to scattering of the secondary electrons at graphene and/or its interfaces with metal and vacuum. One may associate the rather broad α band with the resonant electron transmission through the graphene layer [33], while the sharp β feature is known to be caused by pre-emergent beam effects in electron diffraction [18,43]. This will be discussed further in more detail, involving the computational analysis.

A. Weakly bound graphene

Let us turn now to a system where graphene is only weakly coupled to the substrate, namely to graphene/Au/Ni(111). Intercalation of gold into the graphene/Ni interface allows us

to separate the chemically active $3d$ orbitals of the Ni(111) surface from the C p_z states of graphene making it quasifreestanding [36,44].

In Fig. 2(a), we present a comparison of the computed electron transmission coefficient $T(E, \mathbf{k}_\parallel)$ through a freestanding graphene layer together with the ARPES intensity
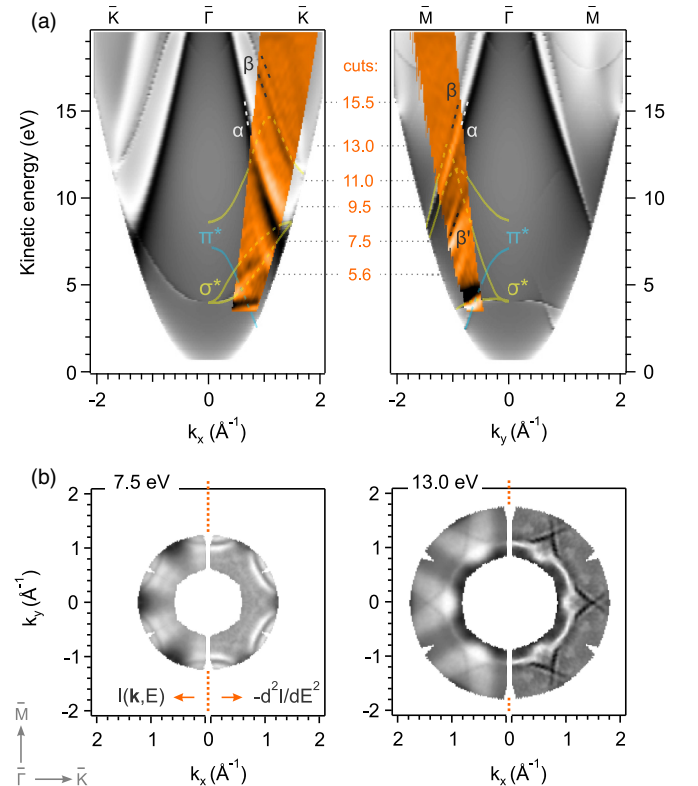
FIG. 2. (a) Comparison of the computed electron transition probability (gray scale) through freestanding graphene with the ARPES data (colored) taken from graphene/Au/Ni(111). Experimental data are shown as a second derivative of as-measured intensity plot. ARPES data were obtained at $h\nu = 68$ eV. The dispersion of $\pi^\star$ and $\sigma^\star$ conductive bands was taken from Ref. [33]. Marked with dotted lines are the levels of constant-energy maps depicted in Figs. 3 and 5. (b) Comparison of the as-measured ARPES data from graphene/Au/Ni(111) with their second-order energy derivative.

obtained from the graphene/Au interface. The experimental photocurrent map and the computed $T(E, \mathbf{k}_\parallel)$ data are shown in orange and gray color schemes, respectively, for the low-kinetic-energy range, where the spectral features caused by the scattered secondary electrons are expected. The dark regions indicate low measured intensity of photoelectrons or low calculated transmission $T(E, \mathbf{k}_\parallel)$. For better contrast, we present the ARPES data as a second derivative of intensity plot with negative sign: $-d^2I/dE^2$. In Fig. 2(b), we show the isoenergy surfaces for the kinetic energies of 7.5 and 13 eV for the as-measured case (left half-maps) and as a second derivative (right half-maps). One can see that the spectral features are much sharper and better seen in the second-derivative maps.

In the theoretical $T(E, \mathbf{k}_\parallel)$ maps in Fig. 2(a), one can distinguish branches of low transmission. The most prominent one, indicated by α, is the scattering resonance due to the quasistationary states embedded into the energy continuum above the vacuum level [33,45]. When electron moves perpendicular to the surface with energy just below the real part of the eigenvalue of such resonance state, it is elastically scattered along the surface and totally reflected. For electrons moving perpendicularly to a freestanding graphene layer, the resonant energy is 27.5 eV [33]. As we can see from Fig. 2(a), the dark branches α of $T(E, \mathbf{k}_\parallel)$ are also prominent away from the $\bar{\Gamma}$ point at lower energies. Their dispersion is in excellent agreement with the very narrow dark bands in the ARPES data within the energy window from 8 to 13 eV. The calculations also predict a rapid variation of $T(E, \mathbf{k}_\parallel)$ in moving across the resonance: A total reflection $T = 0$ abruptly changes to a narrow bright band of $T = 1$, i.e., total transmission of electrons through graphene. Both spectral dips and peaks are expected to be observed experimentally as low and high photoemission intensity in the vicinity of the quasistationary states. In particular, such shape of $T(E, \mathbf{k}_\parallel)$ explains the spectral feature α near the $\bar{\Gamma}$ point in Fig. 1. We also suppose that the "free-electron-like parabolic bands," observed previously in the ARPES spectra of Ref. [17] and angle-resolved secondary electron emission maps of Ref. [35], are actually the features of the secondary electron distribution corresponding to the lines of total transmission. As shown in Ref. [33], the resonance states split into three branches at the $\bar{\Gamma}$ point. The ARPES data in Ref. [17] also reveal a third band passing through the bright cone near 27 eV along the $\bar{\Gamma}\bar{K}$ direction, which is in a good agreement with theoretical prediction. Note that the fit of dispersion $E(k_x, k_y)$ of the resonances by a set of parabolic bands can be done only for the relatively large kinetic energies.

There are a few less intense branches of the calculated $T(E, \mathbf{k}_\parallel)$, which cross the $\bar{\Gamma}$ point at the kinetic energies of 4–9 eV. They coincide with $\pi^\star$ and $\sigma^\star$ states in the conduction band of graphene calculated in the repeated supercell geometry (periodically stacked graphene layers) [33]. For comparison, we show these states with blue and yellow lines in Fig. 2(a). Quasistationary bound states in the conduction band have been predicted to be accompanied by the resonant transmission of secondary electrons passing through a thin layer [46], and they can also act as emission centers populated by the scattered photoelectrons [14,15]. At certain $\mathbf{k}_\parallel$, the resonances may turn into true bound states embedded into the energy continuum [33,45]. In our calculations, $\pi^\star$ and $\sigma^\star$ states of freestanding graphene layer manifest themselves as scattering resonances. We keep referring to the respective features as $\pi^\star$ and $\sigma^\star$ bands for convenience, following the widely used notation. In the experimental data in Fig. 2(a), we can see that the branch of the local maximum of $T(E, \mathbf{k}_\parallel)$ along the $\sigma^\star$ band coincides with the region of enhanced ARPES signal in the window of 4–7 eV along $\bar{\Gamma}\bar{K}$.

The narrow dark features of the calculated distribution $T(E, \mathbf{k}_\parallel)$, marked by β, are shifted to higher energy with respect to the scattering resonances and cross the $\bar{\Gamma}$ point at 33.1 eV. In contrast to the α resonances, the β features do not depend on the details of the electronic structure of the crystal and are determined mainly by the lattice geometry [33,47]. Their energy positions are characterized by the emergence condition for the electron scattered by a reciprocal lattice vector $\mathbf{G}_\parallel$: $E(\mathbf{k}_\parallel) \sim |\mathbf{k}_\parallel + \mathbf{G}_\parallel|^2$. The same effect is observed in LEED as oscillations of the intensity of each diffracted beam just below the emergence threshold of a new nonspecular beam [48–51]. The origin of the fine structure in the I(V) LEED dependences was intensively discussed in the 1970s–80s and can be described by simple models [47,52,53].

In Ref. [30], it was shown that the threshold effects arise from the scattering in the monoatomic overlayer while the substrate plays a minor role. Therefore, the crystalline quality of the surface, its homogeneity, existence of any defects and adsorbates would play a key role in how the threshold phenomena are manifested in $T(E, \mathbf{k}_\parallel)$. The signature of such effects has been recently observed in the photoelectron microscopy [18,43] and spectroscopy measurements [17] as the appearance of the sharp dips of the photoelectron intensity similar to the β structures in Figs. 1 and 2. We also believe that the respective feature marked by β' in Fig. 2(a) has a common origin with β. However, the appearance of β' is caused by the diffraction of the secondary electrons at the Au/graphene interface rather than at the interface with vacuum. The reason for this will become obvious from our further considerations.

The most explicit evidence for the correlation between the calculated distribution $T(E, \mathbf{k}_\parallel)$ and the variations of the emission intensity observed experimentally is seen in Fig. 3, where the isoenergy cuts derived from the ARPES maps and calculations are compared. The positions of these cuts on the energy scale are depicted in Fig. 2(a) by the dotted lines. The horizontal k_x and vertical k_y axes are parallel to the $\bar{\Gamma}\bar{K}$ and $\bar{\Gamma}\bar{M}$ directions, respectively. The comparison of the experimental results for graphene/Au/Ni(111) with the calculations for freestanding graphene is shown in the Figs. 3(a)–3(f). There is a rather good agreement between experiment and theory for all $\mathbf{k}_\parallel$ directions. The most prominent dark feature around the $\bar{\Gamma}$ point together with the neighboring bright area are labeled α, following our previous notation. These peculiarities are characterized by the minimal and maximal transparency of graphene for low-kinetic-energy electrons and are linked to the scattering resonances in the conduction band. Such abrupt changes of the transmission coefficient of graphene are in perfect accord with the general picture of the scattering of low-energy electrons at a flat 2D lattice with quasistationary states in the continuous spectrum.

The narrow β arcs crossing each other in the $\bar{\Gamma}\bar{K}$ directions appear due to the threshold effects in the diffraction of the
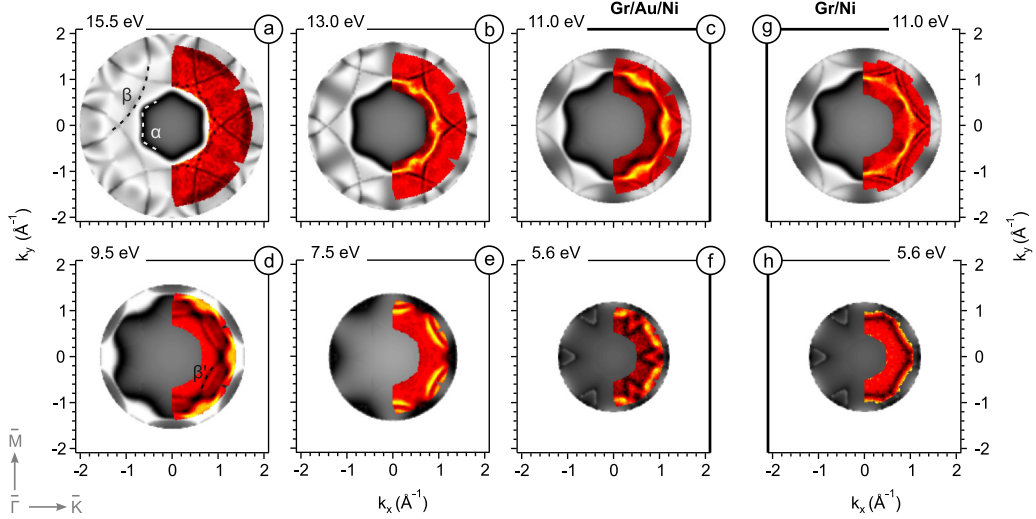
FIG. 3. Constant energy maps of the calculated electron transition probability (gray scale) through graphene compared with the measured 2D emission patterns (colored) of secondary electrons photoexcited from (a)–(f) graphene/Au/Ni(111) and (g), (h) graphene/Ni(111). The 2D emission patterns were taken with 68 eV of photons; second-order energy derivative of data is presented.

secondary electrons at the crystal-vacuum interface. This is why these features are well described by the circles, which are the isoenergy cuts of free-electron-like paraboloids shifted away from the $\bar{\Gamma}$ point by a reciprocal vector of the graphene lattice [17,18]. At low kinetic energies, the α and β features move to the borders of the Brillouin zone in accordance with their dispersion laws [Fig. 2(a)]. At the energies of 9.5 and 7.5 eV, the experimental data reveal a new set of dark β' arcs [Figs. 3(d) and 3(e)]. The β' bands can be described by the free-electron-like paraboloids shifted from the $\bar{\Gamma}$ point by a reciprocal vector of the Au(111) surface. This suggests that the β' features stem from the threshold effect in the diffraction of the secondary electrons at the Au/graphene interface.

Below 7.5 eV, the features originating from the $\pi^{\star}$ and $\sigma^{\star}$ states embedded into the energy continuum of graphene conduction band become visible in the isoenergy cuts of the calculated $T(E, \mathbf{k}_{\parallel})$ [Fig. 3(f)]. The respective structure of T is also reflected in the ARPES maps as wedgelike features along $\bar{\Gamma}\bar{K}$ with varying intensity of photoelectron signal. Such behavior is consistent with the calculations, which predict that the energy dependence of reflection near the quasibound states has the form of a Fano resonance [33,45] with abrupt changes from total reflection to full transparency.

As seen from Fig. 3(f), the most pronounced features in the spectra of secondary electrons at the lowest energies are not determined by the spectral structure of the transmission coefficient of graphene. As will be discussed further, this discrepancy can be explained by the specific angular distribution of the secondary electrons formed in the bulk of the substrate.

B. Tightly bound graphene

As seen from Figs. 2 and 3, there is a good general agreement of the ARPES spectral features of graphene on gold and the theoretical transmission coefficient for free-standing graphene. Then the question arises: How does the angular distribution of secondary electrons change in the case of graphene tightly bound to the substrate, like in

the graphene/Ni system? In Figs. 3(g) and 3(h), we compare the ARPES data for this system with the theoretical $T(E, \mathbf{k}_{\parallel})$ of freestanding graphene. Similarly to the case of freestanding graphene, the dark β arcs are well seen in the secondary electron emission maps of graphene/Ni but the overall spectral pattern of tightly bound graphene differs from that of freestanding graphene and graphene/Au/Ni. Also, in the spectra of both graphene/Ni and graphene/Au/Ni at the lowest energies there are arcs, which are absent in the calculated $T(E, \mathbf{k}_{\parallel})$ for freestanding graphene and, thus, are likely related to the substrate. The latter will become clear from the comparison of the experiment with the calculations of $T(E, \mathbf{k}_{\parallel})$ for graphene on the nickel surface.

Figure 4 shows our calculated transmission spectra for two configurations of graphene on nickel: top-fcc and bridge-top [54,55]. As above, by β we mark the narrow features indicating the drop of the transmitted electron current caused by the threshold diffraction effects. As was discussed earlier for the case of graphene on gold, at low kinetic energies the
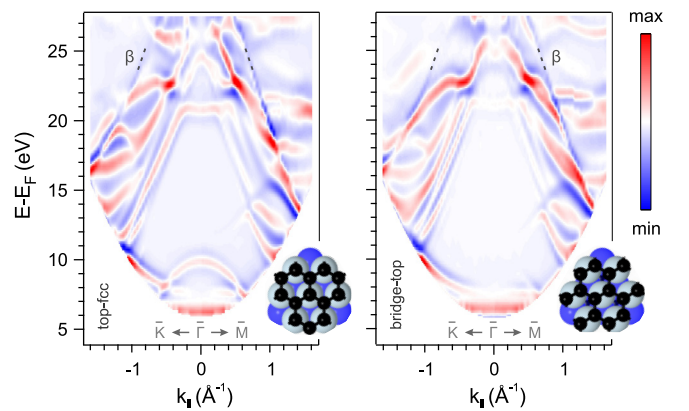

FIG. 4. Comparison of the energy-momentum distribution of the transmitted current for the two configurations of graphene on Ni(111): top-fcc (left) and bridge-top (right).
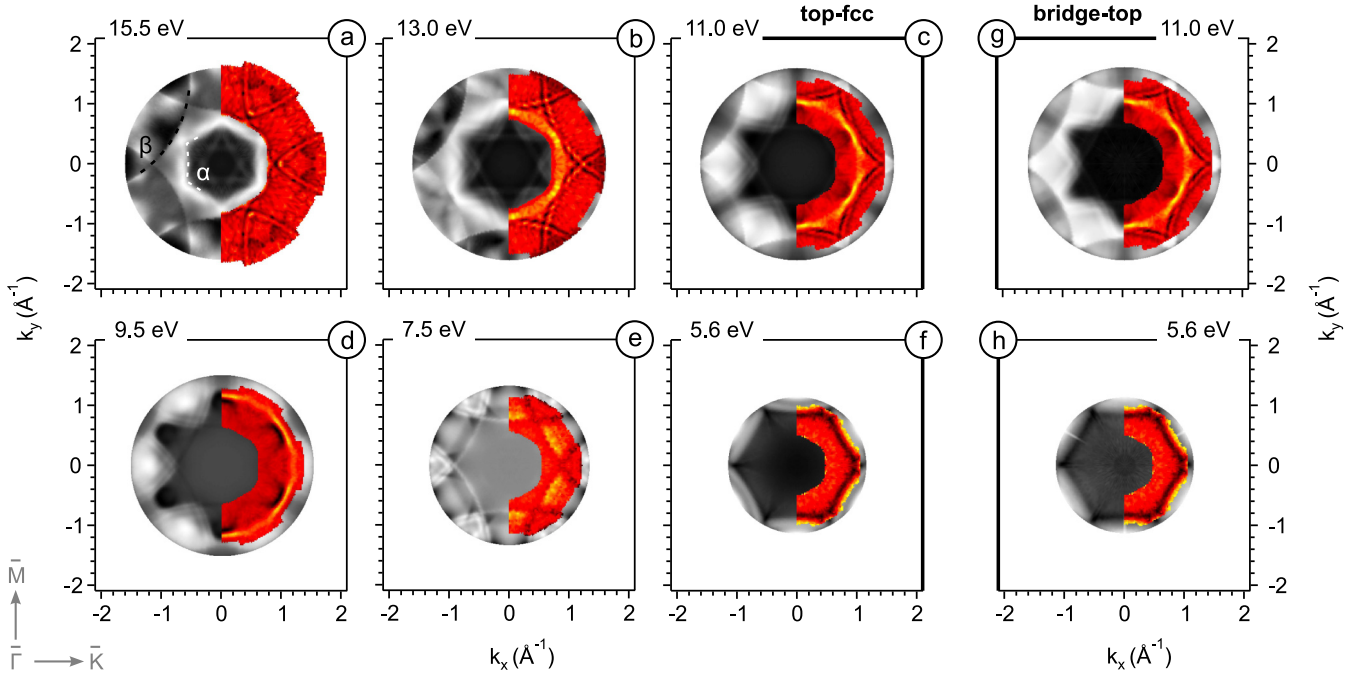
FIG. 5. Measured 2D emission patterns (colored) of secondary electrons photoexcited from graphene/Ni(111) compared to the constant energy maps of electron transition probability (gray scale) through the graphene layer atop Ni(111) in cases of (a)–(f) top-fcc, and (g), (h) bridge-top configurations. 2D emission patterns were obtained at $h\nu = 68$ eV; second-order energy derivative of the data is presented.

dispersions of the $\pi^{\star}$ and $\sigma^{\star}$ bands determine the $E(\mathbf{k}_{\parallel})$ lines along which the graphene's transmittance sharply changes. For the top-fcc configuration [Fig. 4, left], the concave $\pi^{\star}$ band with a maximum at 10 eV above the Fermi level plays an essential role as a current-carrying state, while for the bridge-top configuration this feature vanishes [Fig. 4, right]. The principal difference of the graphene/Ni system from the freestanding graphene is that the strong hybridization of Ni and C electronic states leads to the disappearance of the quite narrow α feature. Instead, a richer structure in the distribution of the transmitted current appears, see Figs. 2(a) and 4.

In Fig. 5, we compare the experimental and theoretical results for the graphene/Ni system for energies between 5.6 and 15.5 eV above the vacuum level. At the lowest energies, the calculated $T(E, \mathbf{k}_{\parallel})$ for tightly bound graphene agrees well with the ARPES-derived secondary electron emission pattern from graphene/Ni. Our calculation describes successfully both dark and bright arcs at 5.6 and 7.5 eV. These features are solely determined by the transmission properties of the nickel substrate, as they are absent in the calculated distribution of $T(E, \mathbf{k}_{\parallel})$ for freestanding graphene. At relatively high kinetic energies closer to the $\bar{\Gamma}$ point, one can resolve a sequence of the alternating regions of resonant reflection and resonant transmission of electrons through graphene. Our calculations reveal a fine structure of such regions, which are not perfectly resolved in the experiment, but the positions of these areas and their contours are very well seen for the kinetic energies above 7.5 eV. Closer to the edges of the Brillouin zone, at higher energies, one can distinguish the β arcs stemming from the threshold effects.

Our theory describes the overall ARPES spectrum quite well. However, there is a small mismatch between measured and calculated positions of the α and β features at higher

energies. For example, the dark edge of the α-contour at 9.5 and 11 eV and the bright one at 13 eV are closer to the $\bar{\Gamma}$ point in the ARPES-derived secondary electron emission maps [Figs. 5(b)–5(d)]. The same is true for the β arcs, see Figs. 5(a) and 5(b). Above 9 eV, we find that the calculated energy cuts are shifted to higher energies by ~1 eV relative to the experiment, see Fig. 6. Such a stretching of the theoretical spectrum relative to the experiment is not a typical result of using the Kohn-Sham quasiparticles for final states. We tentatively ascribe the discrepancy to the uncertainty of the crystal potential at the interface, which may be caused by small errors in the geometry of the overlayer assumed in the theory or by an uncertainty in the charge transfer between the substrate and graphene overlayer in the ground-state calculation.

C. The role of bulk substrate

In Fig. 7, we compare the secondary electron emission distributions for clean (left half-maps) Ni(111) and Au/Ni(111) with those for graphene-covered (right half-maps) surfaces. There is a rather moderate difference between Ni(111) and graphene/Ni(111) in the spectral patterns at 5.6 and 6.5 eV, see Figs. 7(e) and 7(f). The only difference is along the $\bar{\Gamma}\bar{K}$ lines at the corners of a dark hexagon formed by crossing arcs. For the graphene-capped system, additional features can be seen in these corners in agreement with the calculated transmitted current, see Fig. 5(f). With the increase of kinetic energy, the fine structure of the graphene's transmission coefficient becomes better and better resolved.

The differences in the emission patterns for clean and graphene-coated Au/Ni substrates are more pronounced than in the systems without gold, see Figs. 7(a) and 7(e). This can be explained by the resonant changes of the graphene's
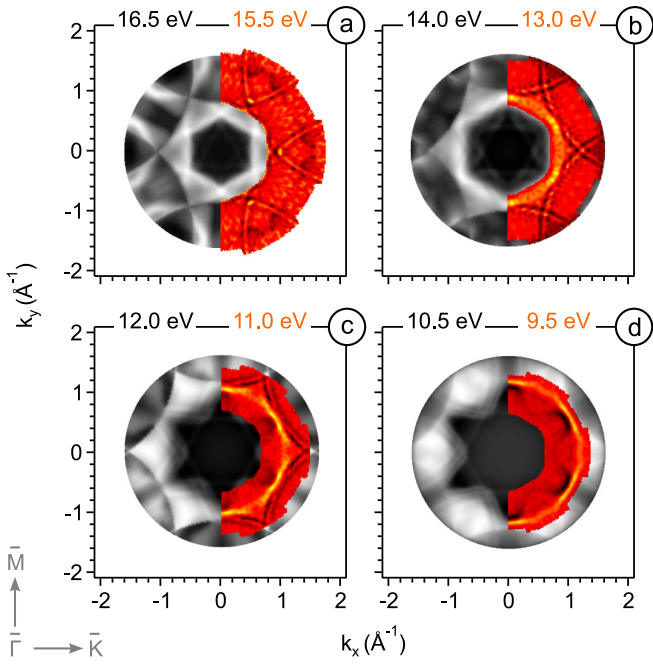
FIG. 6. Measured 2D emission patterns (colored) of secondary electrons photoexcited from graphene/Ni(111) compared to $T(E, \mathbf{k}_\parallel)$ (gray scale) calculated for top-fcc configuration. Corresponding cuts of the theoretical maps were taken at higher kinetic energies with respect to the experimental data. The kinetic energy of the theoretical spectrum is indicated on the left and of the measured one on the right of the respective graph.

transmission in the vicinity of the $\sigma^\star$ bands. Due to the strong coupling of graphene to the substrate, the conduction band states of graphene/Ni are shifted down by about 1–2 eV relative to those of freestanding graphene. Thus, for the same energy, the $\sigma^\star$-related feature appears at different $\mathbf{k}_\parallel$.

For graphene/Au, it is closer to the $\bar{\Gamma}$ point. Therefore, its contribution to the spectral pattern of secondary electrons is more pronounced for weakly coupled graphene at the energies below 7 eV.

For the energy of 7.5 eV along the $\bar{\Gamma}\bar{M}$ direction for Au/Ni and graphene/Au/Ni, there appear dark arcs due to the threshold effects associated with the electron scattering by a reciprocal vector of the Au layer at the graphene/Au interface (β' features). At 9.8 eV, the same effect coming from the crystal/vacuum interface is observed (β arcs). Because of the small mismatch (less than 2%) in the lattice parameters of Ni(111) and graphene, the positions of the β arcs are nearly identical for these systems. At higher energies for the graphene-covered surfaces, the most pronounced features in the spectra of secondary electrons are determined by the spectral structure of the transmission coefficient of graphene.

The ARPES images at the lowest kinetic energies look rather similar for Ni and Au/Ni systems. The most pronounced features there are the dark and bright arcs, which shift to the $\bar{\Gamma}$ point with increasing kinetic energy of electrons. These arcs are absent in the calculated $T(E, \mathbf{k}_\parallel)$ for freestanding graphene, but they appear when graphene is deposited on Ni(111). Apparently, these features are related to the bulk of the Ni substrate.

IV. CONCLUSIONS

We performed experimental and theoretical studies of the fine structure of the ARPES spectra originating from the secondary electron emission from graphene-covered surfaces. The secondary electron features are seen as a set of dark and bright arcs and cones superimposed on the spectral map of the primary photoelectrons. We explored two systems: graphene/Au/Ni and graphene/Ni. Graphene on gold is freestandinglike, while on nickel it is tightly bound to the
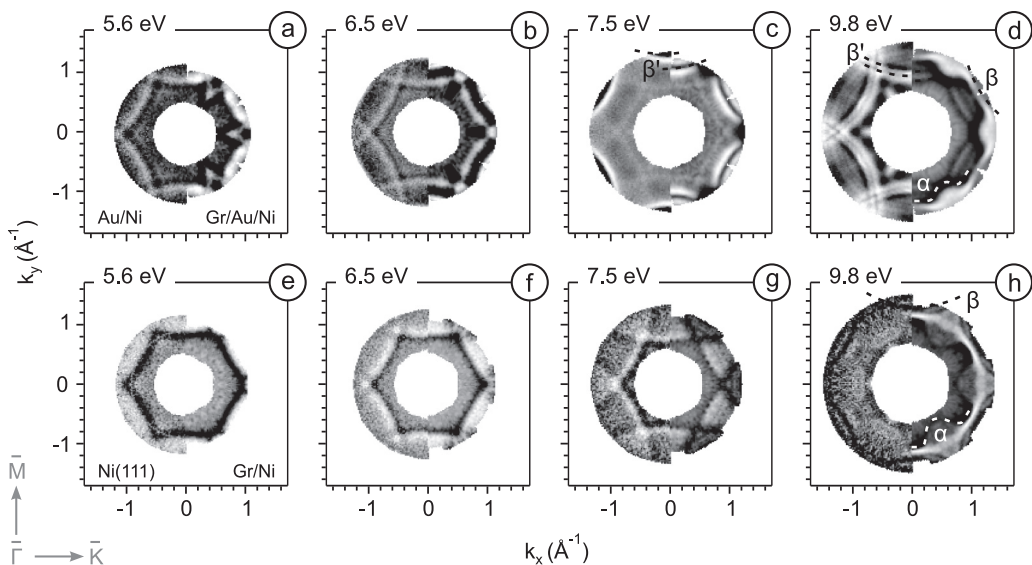

FIG. 7. 2D emission patterns of secondary electrons photoexcited from (a)–(d) graphene/Au/Ni(111) and (e)–(h) graphene/Ni(111) compared to that from the respective metallic substrates: Au/Ni(111) and Ni(111). The data were taken with 68 eV of photons for the graphene-based systems, and with 21.2 eV of photons for clean metallic substrates. The results are shown as a second derivative of the as-measured ARPES data.

substrate. Since the metallic substrate itself influences the secondary electron spectra, the ARPES measurements were performed for the respective bare metallic systems, too.

To interpret the experimental data, we calculated the graphene's transmission coefficient $T(E, \mathbf{k}_\parallel)$, which is closely related to the angular distribution of secondary electrons. The calculations reveal two types of features—α and β—in the energy-angular distribution of electron transmission. The α features depend on the structure of the conduction band of graphene and reflect the quasistationary states (resonances) embedded into the energy continuum. Around the resonance the transmission coefficient rapidly changes from maximum to minimum. As a result, a well-defined structure appears in the secondary electron emission spectra, and the dispersion of the resonances α can be measured in the ARPES experiment. The β features signify the emergence of the secondary diffracted beams in vacuum. Their dispersion is determined by the surface reciprocal lattice $\mathbf{G}_\parallel$. In contrast to the resonances α, the β features do not depend on the details of the electronic structure and are observed in the spectra taken from both the bare and graphene-covered metallic substrates. On the other hand, the α features do not appear in the spectra of the graphene-free surfaces. We have also found that for the kinetic energies below 8 eV, the distribution of graphene's $T(E, \mathbf{k}_\parallel)$ contains no sharp structures over a wide $\mathbf{k}_\parallel$-region around the $\bar{\Gamma}$ point, and, thus, the ARPES maps mainly reflect the structure of the secondary electron emission spectra of the substrate.

Our study demonstrates that secondary electrons carry important complementary information about unoccupied electronic structure, which in the spectra of primary electrons is blurred by the highly selective optical transitions. The enhanced surface sensitivity of secondary emission makes it especially useful for studies of thin overlayers. Good agreement between the *ab initio* calculations and experimentally obtained secondary electron emission maps, indicates that our approach can be successfully applied to the analysis of electron transmission properties of Q2D materials.

[1] G. R. Bhimanapati, Z. Lin, V. Meunier, Y. Jung, J. Cha, S. Das, D. Xiao, Y. Son, M. S. Strano, V. R. Cooper, L. Liang, S. G. Louie, E. Ringe, W. Zhou, S. S. Kim, R. R. Naik, B. G. Sumpter, H. Terrones, F. Xia, Y. Wang, J. Zhu, D. Akinwande, N. Alem, J. A. Schuller, R. E. Schaak, M. Terrones, and J. A. Robinson, Recent advances in two-dimensional materials beyond graphene, ACS Nano **9**, 11509 (2015).

[2] H. Zhang, Ultrathin two-dimensional nanomaterials, ACS Nano **9**, 9451 (2015).

[3] K. S. Novoselov, V. I. Fal'ko, L. Colombo, P. R. Gellert, M. G. Schwab, and K. Kim, A roadmap for graphene, Nature **490**, 192 (2012).

[4] Y. Liu, N. O. Weiss, X. Duan, H.-C. Cheng, Y. Huang, and X. Duan, Van der Waals heterostructures and devices, Nat. Rev. Mater. **1**, 16042 (2016).

[5] K. S. Novoselov, A. Mishchenko, A. Carvalho, and A. H. Castro Neto, 2D materials and van der Waals heterostructures, Science **353**, aac9439 (2016).

[6] B. Liu, A. Abbas, and C. Zhou, Two-dimensional semiconductors: From materials preparation to electronic applications, Adv. Electron. Mater. **3**, 1700045 (2017).

[7] R. Frisenda, A. J. Molina-Mendoza, T. Mueller, A. Castellanos-Gomez, and H. S. J. van der Zant, Atomically thin p-n junctions based on two-dimensional materials, Chem. Soc. Rev. **47**, 3339 (2018).

[8] C. Hwang, D. A. Siegel, S.-K. Mo, W. Regan, A. Ismach, Y. Zhang, A. Zettl, and A. Lanzara, Fermi velocity engineering in graphene by substrate modification, Sci. Rep. **2**, 590 (2012).

[9] A. V. Fedorov, N. I. Verbitskiy, D. Haberer, C. Struzzi, L. Petaccia, D. Usachov, O. Y. Vilkov, D. V. Vyalikh, J. Fink, M. Knupfer, B. Büchner, and A. Grüneis, Observation of a universal donor-dependent vibrational mode in graphene, Nat. Commun. **5**, 3257 (2014).

[10] D. Usachov, A. Fedorov, M. M. Otrokov, A. Chikina, O. Vilkov, A. Petukhov, A. G. Rybkin, Y. M. Koroteev, E. V. Chulkov, V. K. Adamchuk, A. Grüneis, C. Laubschat, and D. V. Vyalikh, Observation of single-spin Dirac fermions at the graphene/ferromagnet interface, Nano Lett. **15**, 2396 (2015).

[11] D. Usachov, A. Fedorov, O. Vilkov, B. Senkovskiy, V. K. Adamchuk, L. V. Yashina, A. A. Volykhov, M. Farjam, N. I. Verbitskiy, A. Grüneis, C. Laubschat, and D. V. Vyalikh, The chemistry of imperfections in N-graphene, Nano Lett. **14**, 4982 (2014).

[12] A. Bostwick, T. Ohta, T. Seyller, K. Horn, and E. Rotenberg, Quasiparticle dynamics in graphene, Nat. Phys. **3**, 36 (2006).

[13] A. R. Law, J. J. Barry, and H. P. Hughes, Angle-resolved photoemission and secondary electron emission from single-crystal graphite, Phys. Rev. B **28**, 5332 (1983).

[14] T. Takahashi, H. Tokailin, and T. Sagawa, Angle-resolved ultraviolet photoelectron spectroscopy of the unoccupied band structure of graphite, Phys. Rev. B **32**, 8317 (1985).

[15] A. R. Law, M. T. Johnson, and H. P. Hughes, Synchrotron-radiation-excited angle-resolved photoemission from single-crystal graphite, Phys. Rev. B **34**, 4289 (1986).

[16] S. K. Mahatha, K. S. R. Menon, and T. Balasubramanian, Unoccupied electronic structure of graphite probed by angle-resolved photoemission spectroscopy, Phys. Rev. B **84**, 113106 (2011).

[17] M. Krivenkov, D. Marchenko, J. Sánchez-Barriga, O. Rader, and A. Varykhalov, Suppression of electron scattering resonances in graphene by quantum dots, Appl. Phys. Lett. **111**, 161605 (2017).

[18] A. Zaporozhchenko-Zymaková, D. Kutnyakhov, K. Medjanik, C. Tusche, O. Fedchenko, S. Chernov, M. Ellguth, S. A. Nepijko, H. J. Elmers, and G. Schönhense, Momentum-resolved photoelectron absorption in surface barrier scattering on Ir(111) and graphene/Ir(111), Phys. Rev. B **96**, 155108 (2017).

[19] I. Schäfer, M. Schlüter, and M. Skibowski, Conduction-band structure of graphite studied by combined angle-resolved inverse photoemission and target current spectroscopy, Phys. Rev. B **35**, 7663 (1987).

[20] J.-V. Peetz, W. Schattke, H. Carstensen, R. Manzke, and M. Skibowski, Analysis of target-current-spectroscopy data of GaAs(110) with very-low-energy electron-diffraction calculations, Phys. Rev. B **46**, 10127 (1992).

[21] V. N. Strocov, H. I. Starnberg, P. O. Nilsson, H. E. Brauer, and L. J. Holleboom, New Method for Absolute Band Structure Determination by Combining Photoemission with Very-Low-Energy Electron Diffraction: Application to Layered VSe_2, Phys. Rev. Lett. **79**, 467 (1997).

[22] V. N. Strocov, P. Blaha, H. I. Starnberg, M. Rohlfing, R. Claessen, J.-M. Debever, and J.-M. Themlin, Three-dimensional unoccupied band structure of graphite: Very-low-energy electron diffraction and band calculations, Phys. Rev. B **61**, 4994 (2000).

[23] K. Hiraoka and M. Nara, Conduction band structure of solid n-alkanes studied by electron-transmission spectra, Chem. Phys. Lett. **94**, 589 (1983).

[24] M. Pisarra, P. Riccardi, A. Sindona, A. Cupolillo, N. Ligato, C. Giallombardo, and L. Caputi, Probing graphene interfaces with secondary electrons, Carbon **77**, 796 (2014).

[25] F. Wicki, J.-N. Longchamp, T. Latychevskaia, C. Escher, and H.-W. Fink, Mapping unoccupied electronic states of freestanding graphene by angle-resolved low-energy electron transmission, Phys. Rev. B **94**, 075424 (2016).

[26] H. Hibino, H. Kageshima, and M. Nagase, Epitaxial few-layer graphene: Towards single crystal growth, J. Phys. D: Appl. Phys. **43**, 374005 (2010).

[27] R. M. Feenstra, N. Srivastava, Q. Gao, M. Widom, B. Diaconescu, T. Ohta, G. L. Kellogg, J. T. Robinson, and I. V. Vlassiouk, Low-energy electron reflectivity from graphene, Phys. Rev. B **87**, 041406(R) (2013).

[28] H. Hibino, S. Wang, C. M. Orofeo, and H. Kageshima, Growth and low-energy electron microscopy characterizations of graphene and hexagonal boron nitride, Prog. Cryst. Growth Charact. Mater. **62**, 155 (2016).

[29] J. Jobst, A. J. H. van der Torren, E. E. Krasovskii, J. Balgley, C. R. Dean, R. M. Tromp, and S. J. van der Molen, Quantifying electronic band interactions in van der Waals materials using angle-resolved reflected-electron spectroscopy, Nat. Commun. **7**, 13621 (2016).

[30] E. E. Krasovskii, J. Höcker, J. Falta, and J. I. Flege, Surface resonances in electron reflection from overlayers, J. Phys.: Condens. Matter **27**, 035501 (2015).

[31] J.-N. Longchamp, T. Latychevskaia, C. Escher, and H.-W. Fink, Low-energy electron transmission imaging of clusters on free-standing graphene, Appl. Phys. Lett. **101**, 113117 (2012).

[32] C. Li, M. T. Cole, W. Lei, K. Qu, K. Ying, Y. Zhang, A. R. Robertson, J. H. Warner, S. Ding, X. Zhang, B. Wang, and W. I. Milne, Highly electron transparent graphene for field emission triode gates, Adv. Funct. Mater. **24**, 1218 (2014).

[33] V. U. Nazarov, E. E. Krasovskii, and V. M. Silkin, Scattering resonances in two-dimensional crystals with application to graphene, Phys. Rev. B **87**, 041405(R) (2013).

[34] Y. Ueda, Y. Suzuki, and K. Watanabe, Time-dependent first-principles study of angle-resolved secondary electron emission from atomic sheets, Phys. Rev. B **97**, 075406 (2018).

[35] H. Hibino, H. Kageshima, F.-Z. Guo, F. Maeda, M. Kotsugi, and Y. Watanabe, Two-dimensional emission patterns of secondary electrons from graphene layers formed on SiC(0001), Appl. Surf. Sci. **254**, 7596 (2008).

[36] A. Varykhalov, J. Sánchez-Barriga, A. M. Shikin, C. Biswas, E. Vescovo, A. Rybkin, D. Marchenko, and O. Rader, Electronic and Magnetic Properties of Quasifreestanding Graphene on Ni, Phys. Rev. Lett. **101**, 157601 (2008).

[37] D. Nobis, M. Potenz, D. Niesner, and T. Fauster, Image-potential states of graphene on noble-metal surfaces, Phys. Rev. B **88**, 195435 (2013).

[38] D. Niesner and T. Fauster, Image-potential states and work function of graphene, J. Phys.: Condens. Matter **26**, 393001 (2014).

[39] R. Feder and J. B. Pendry, Theory of secondary electron emission, Solid State Commun. **26**, 519 (1978).

[40] M. Bovet, V. N. Strocov, F. Clerc, C. Koitzsch, D. Naumović, and P. Aebi 1, Excited States Mapped by Secondary Photoemission, Phys. Rev. Lett. **93**, 107601 (2004).

[41] V. N. Strocov, E. E. Krasovskii, W. Schattke, N. Barrett, H. Berger, D. Schrupp, and R. Claessen, Three-dimensional band structure of layered $TiTe_2$: Photoemission final-state effects, Phys. Rev. B **74**, 195125 (2006).

[42] E. E. Krasovskii, Augmented-plane-wave approach to scattering of Bloch electrons by an interface, Phys. Rev. B **70**, 245322 (2004).

[43] A. Winkelmann, M. Ellguth, C. Tusche, A. A. Ünal, J. Henk, and J. Kirschner, Momentum-resolved photoelectron interference in crystal surface barrier scattering, Phys. Rev. B **86**, 085427 (2012).

[44] A. M. Shikin, G. V. Prudnikova, V. K. Adamchuk, F. Moresco, and K.-H. Rieder, Surface intercalation of gold underneath a graphite monolayer on Ni(111) studied by angle-resolved photoemission and high-resolution electron-energy-loss spectroscopy, Phys. Rev. B **62**, 13202 (2000).

[45] G. V. Wolf and Y. P. Chuburin, Fano resonances in low-energy electron transmission through crystalline films, J. Phys.: Condens. Matter **21**, 185007 (2009).

[46] G. V. Wolf and Y. P. Chuburin, Specific features of low-energy electron scattering by thin films of cubic crystals, Phys. Solid State **47**, 1048 (2005).

[47] J. C. Le Bosse, J. Lopez, C. Gaubert, Y. Gauthier, and R. Baudoing, A general picture of threshold effects in LEED, J. Phys. C: Solid State Phys. **15**, 6087 (1982).

[48] D. S. Boudreaux and V. Heine, Band structure treatment of low energy electron diffraction intensities, Surf. Sci. **8**, 426 (1967).

[49] E. G. McRae and C. W. Caldwell, Observation of multiple scattering resonance effects in low energy electron

diffraction studies of LiF, NaF and graphite, Surf. Sci. **7**, 41 (1967).

[50] S. Andersson, Resonances in low-energy electron diffraction from the copper (001) surface, Surf. Sci. **19**, 21 (1970).

[51] A. Adnot and J. D. Carette, High-Resolution Study of Low-Energy-Electron-Diffraction Threshold Effects on W(001) Surface, Phys. Rev. Lett. **38**, 1084 (1977).

[52] E. G. McRae, Electronic surface resonances of crystals, Rev. Mod. Phys. **51**, 541 (1979).

[53] C. Gaubert, R. Baudoing, Y. Gauthier, and J. Rundgren, General aspects of beam threshold effects in LEED, Surf. Sci. **147**, 162 (1984).

[54] M. Fuentes-Cabrera, M. I. Baskes, A. V. Melechko, and M. L. Simpson, Bridge structure for the graphene/Ni(111) system: A first principles study, Phys. Rev. B **77**, 035405 (2008).

[55] F. Bianchini, L. L. Patera, M. Peressi, C. Africh, and G. Comelli, Atomic scale identification of coexisting graphene structures on Ni(111), J. Phys. Chem. Lett. **5**, 467 (2014).